

Supplement of Atmos. Chem. Phys., 18, 3119–3145, 2018
<https://doi.org/10.5194/acp-18-3119-2018-supplement>
© Author(s) 2018. This work is distributed under
the Creative Commons Attribution 4.0 License.



Supplement of

Aerosol–cloud interactions in mixed-phase convective clouds – Part 1: Aerosol perturbations

Annette K. Miltenberger et al.

Correspondence to: Annette K. Miltenberger (a.miltenberger@leeds.ac.uk)

The copyright of individual parts of the supplement might differ from the CC BY 4.0 License.

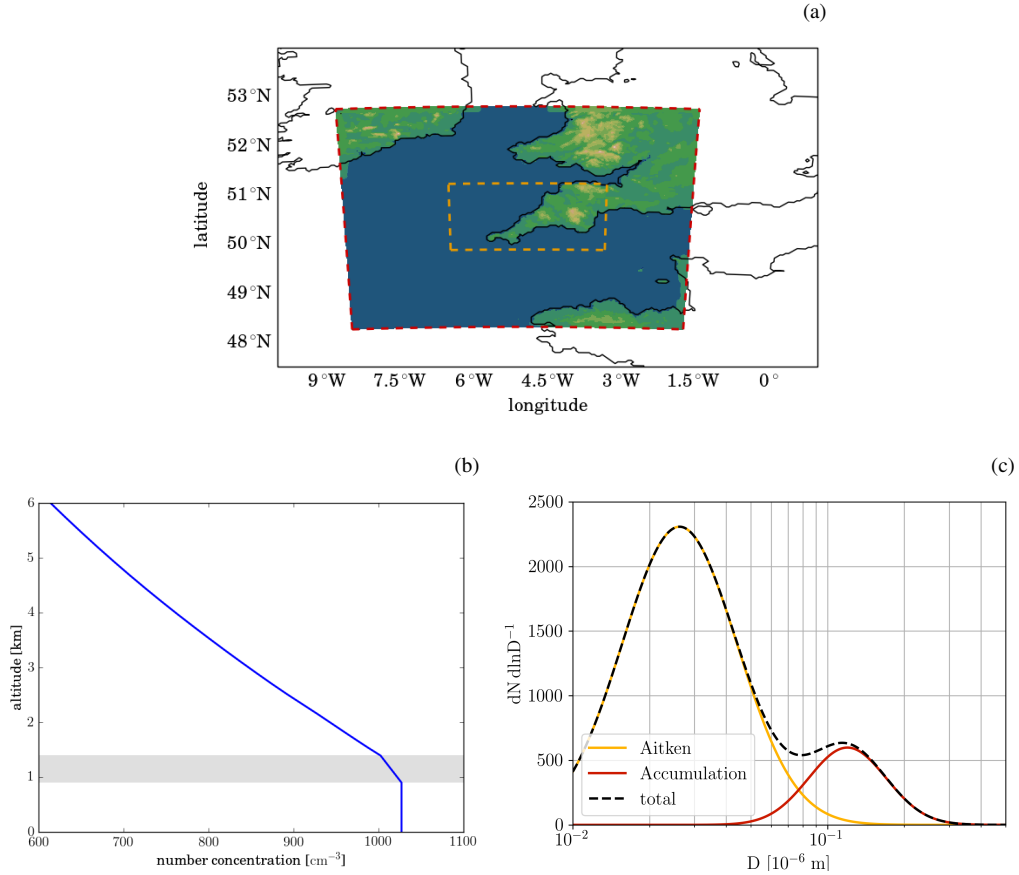


Figure 1. (a) Regional model domains used for the simulations: the red dashed line corresponds to the domain boundary used for the 1 km simulations and the orange dashed line to the one for the 250 m simulation. (b) Aerosol size distribution used for initialising the simulations in the boundary layer: Aitken mode (orange line), accumulation mode (red line) and the sum of both (black dashed line). (c) Vertical profile of the total aerosol number density. The grey horizontal bar shows the 500 m interval around the mean height of the boundary layer, across which a linear decrease of boundary layer aerosol concentrations to free tropospheric concentrations is prescribed.

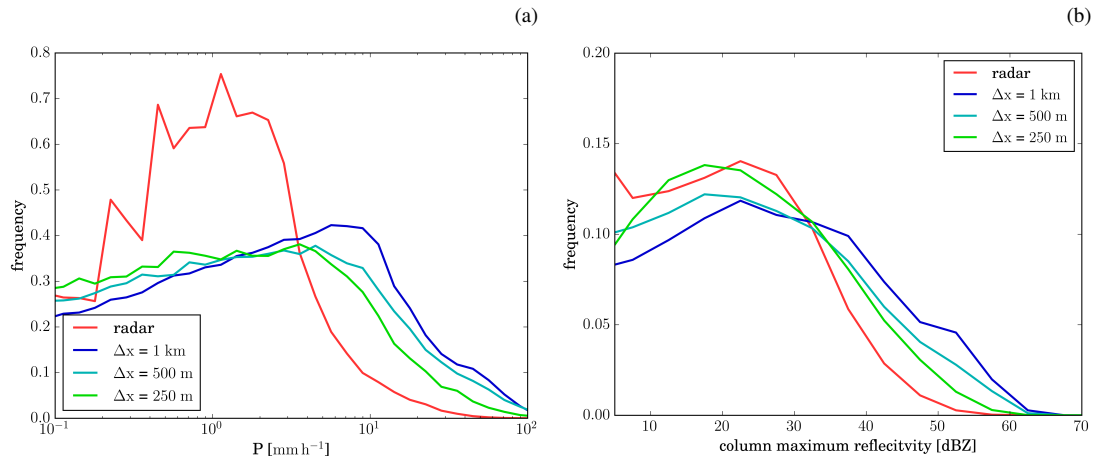


Figure 2. Comparison of the distribution of (a) surface precipitation rate and (b) column maximum radar reflectivity at 750 m from model simulations with different grid spacings (cold colours) and radar observations (red). Simulated precipitation rates and radar reflectivity have been coarse-grained to the spatial resolution of the radar observations (1 km horizontal and 500 m vertical).

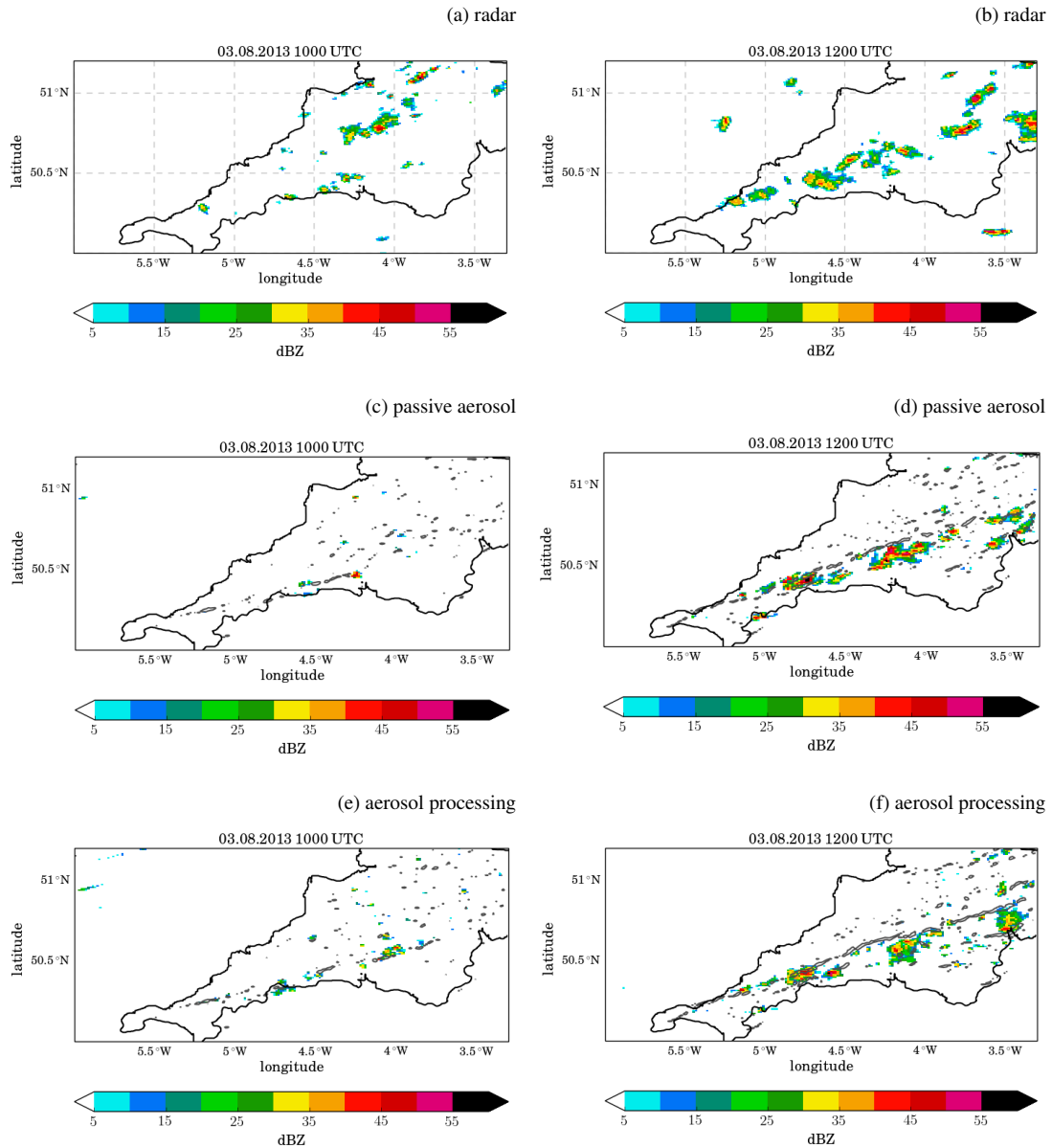


Figure 3. Column maximum radar reflectivity over the COPE domain at 10 UTC (a, c, e) and 12 UTC (b, d, f) from the operational radar network (a, b), the model simulations with passive aerosol (c, d), and with aerosol processing (e, f). The grey contour line indicates regions with convergence larger than $2 \cdot 10^{-6} \text{ s}^{-1}$ at 250 m above ground.

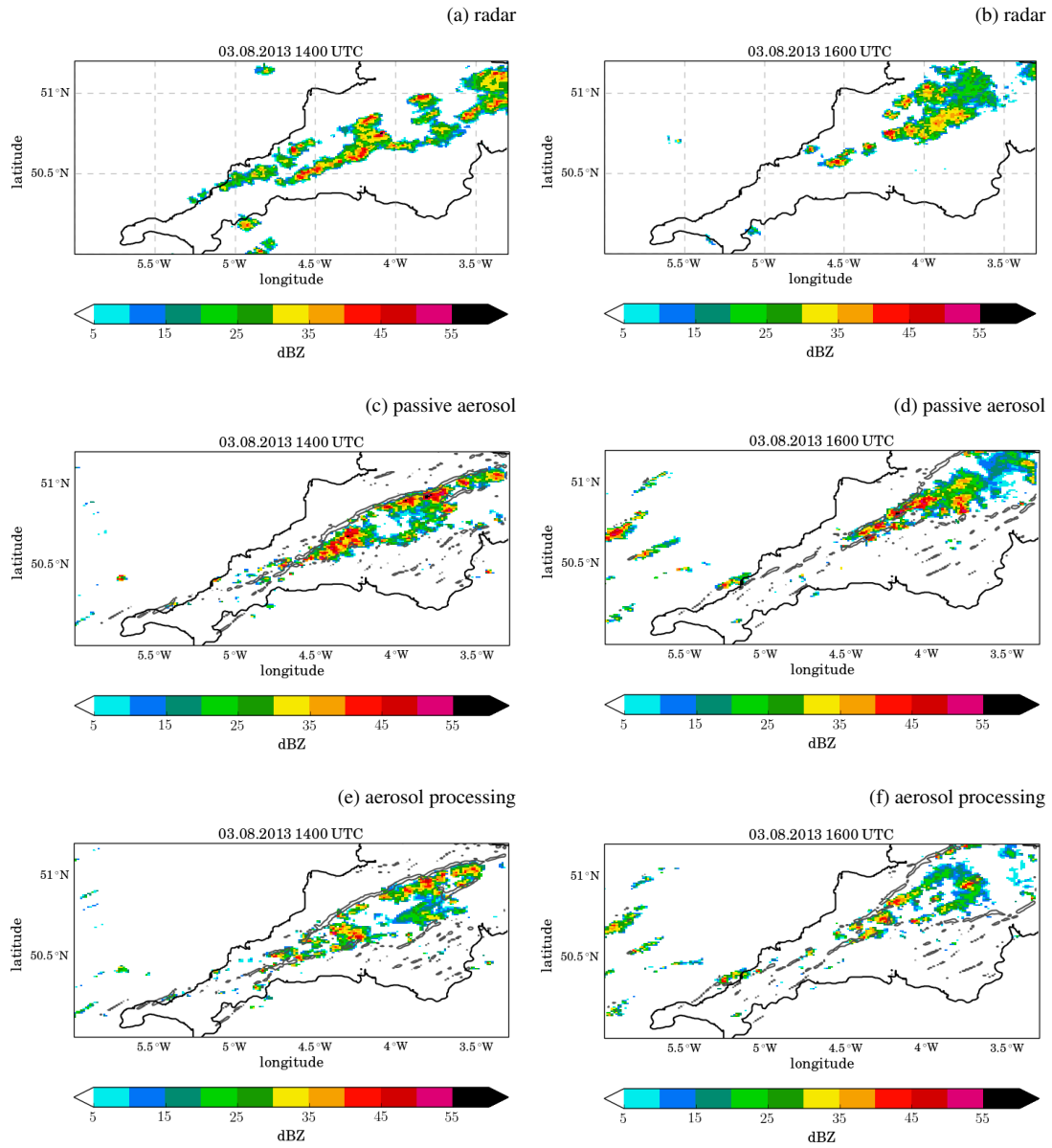


Figure 4. Same as SI Fig. 3 but for 14 UTC (a, c, e) and 16 UTC (b, d, f).

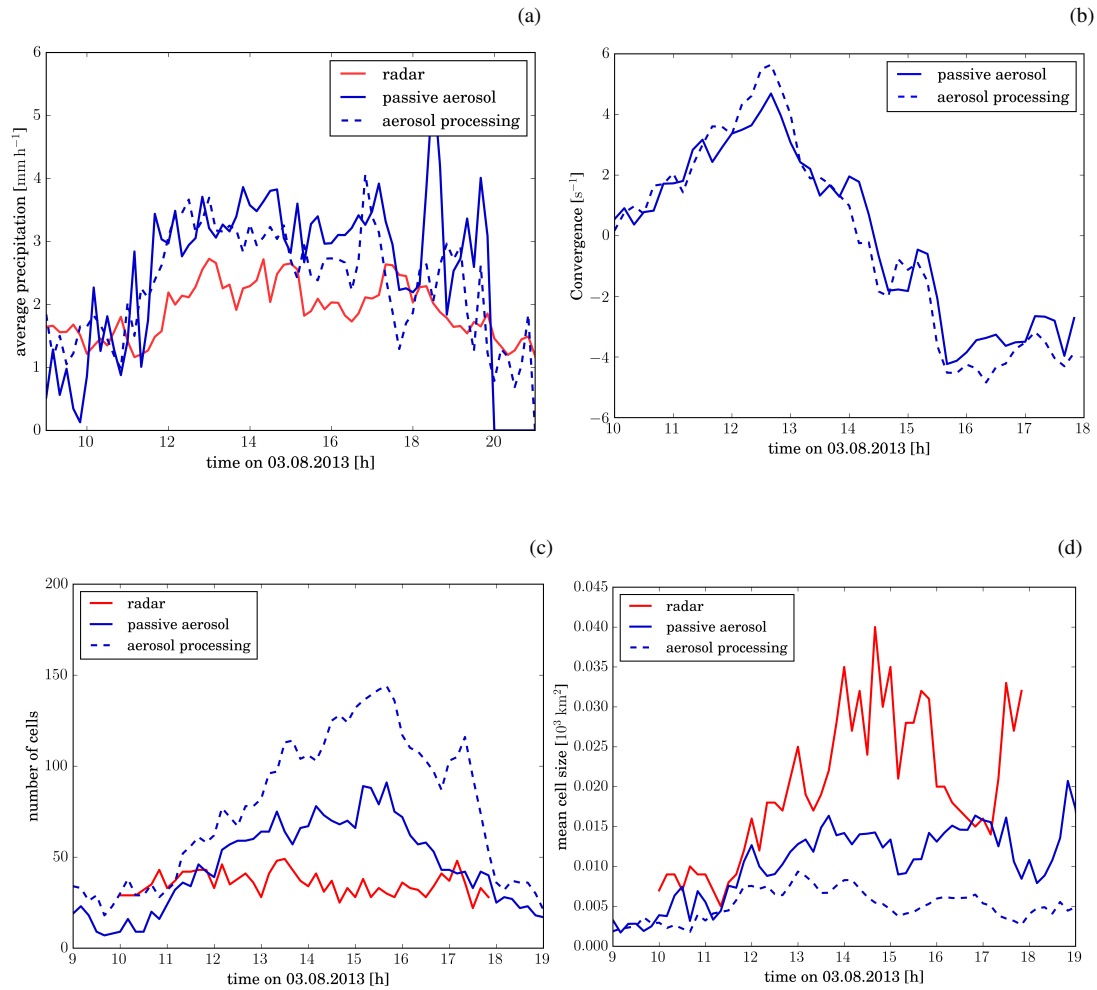


Figure 5. (a) Comparison of the distribution of average precipitation rate for grid points with non-zero precipitation. (b) Timeseries of domain integrated convergence at 250 m above ground for the simulations with the standard aerosol scenario. (c) Cell number and (d) mean cell size from radar observations (red) and model simulations with passive aerosols (solid line) and aerosol processing (dashed line), respectively. Simulated precipitation rates have been coarse-grained to the spatial resolution of the radar observations (1 km horizontal). Cells are defined as continuous regions with column maximum reflectivity larger than 25 dBZ.

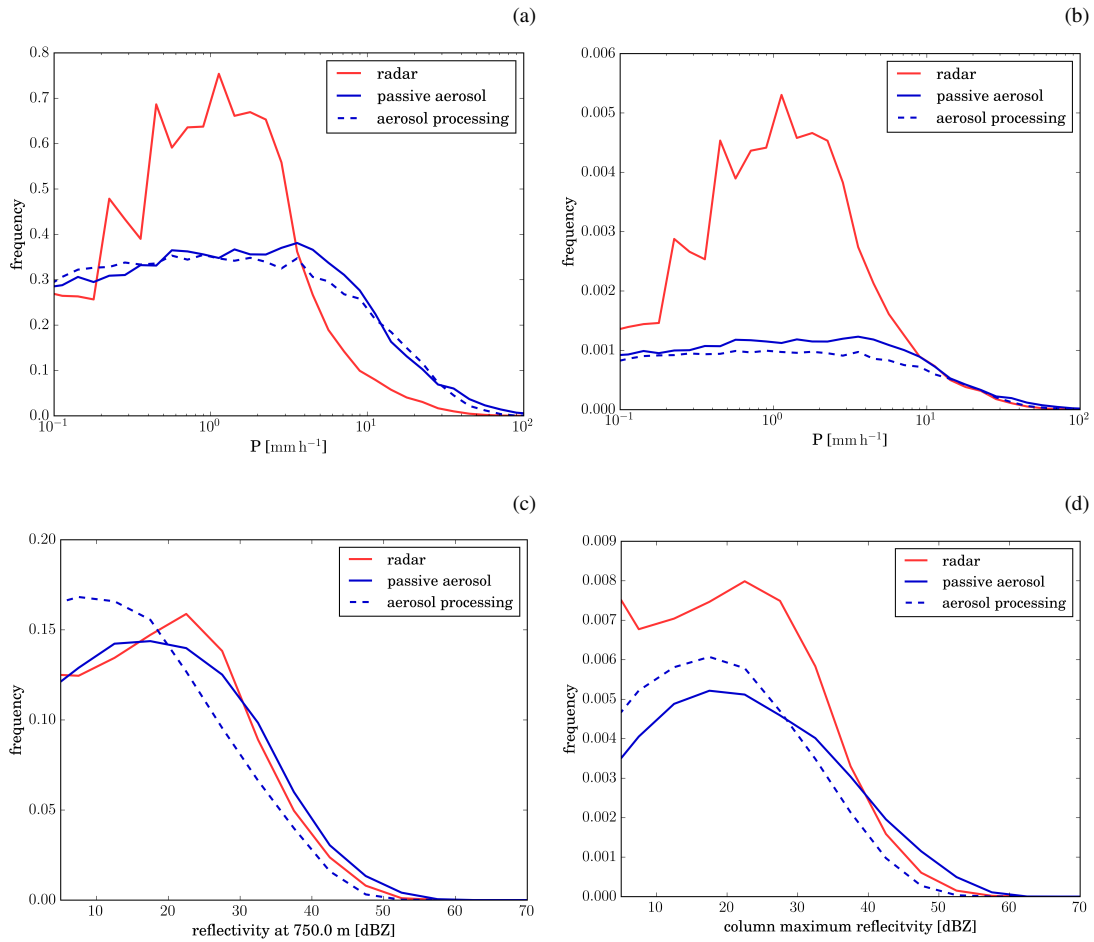


Figure 6. Distribution of surface precipitation rate for (a) gridpoints with surface precipitation and (b) all grid points. (c) Distribution of radar reflectivity at 750 m computed over grid points with reflectivity larger than 0 dBZ. Radar data is shown in red and model data in blue. (d) Distribution of column maximum radar reflectivity computed over all grid points. The solid line shows results from the simulation with passive aerosols and the dashed line from the simulation with aerosol processing. Simulated precipitation rates and radar reflectivity have been coarse-grained to the spatial resolution of the radar observations (1 km horizontal and 500 m vertical).

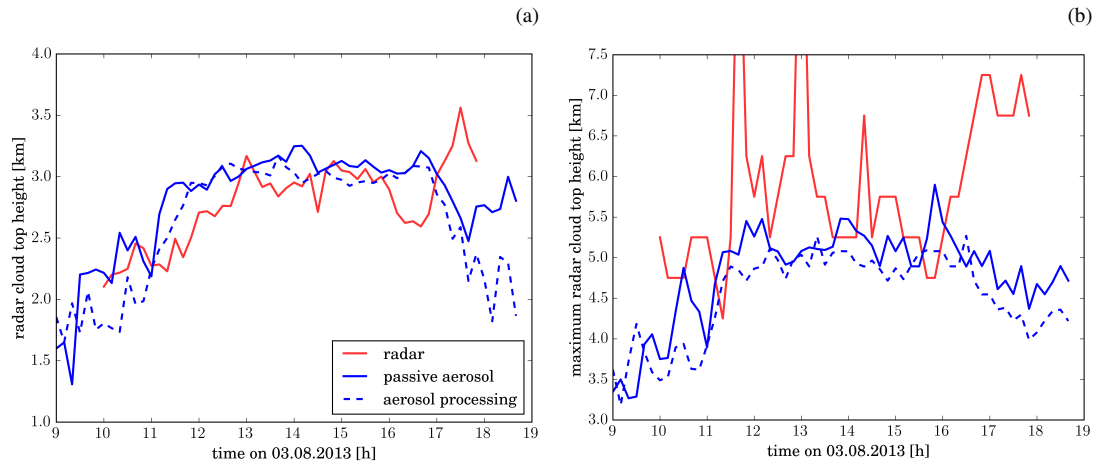


Figure 7. Comparison of (a) domain mean and (b) maximum height of the 18 dBZ contour from model simulations and radar data.

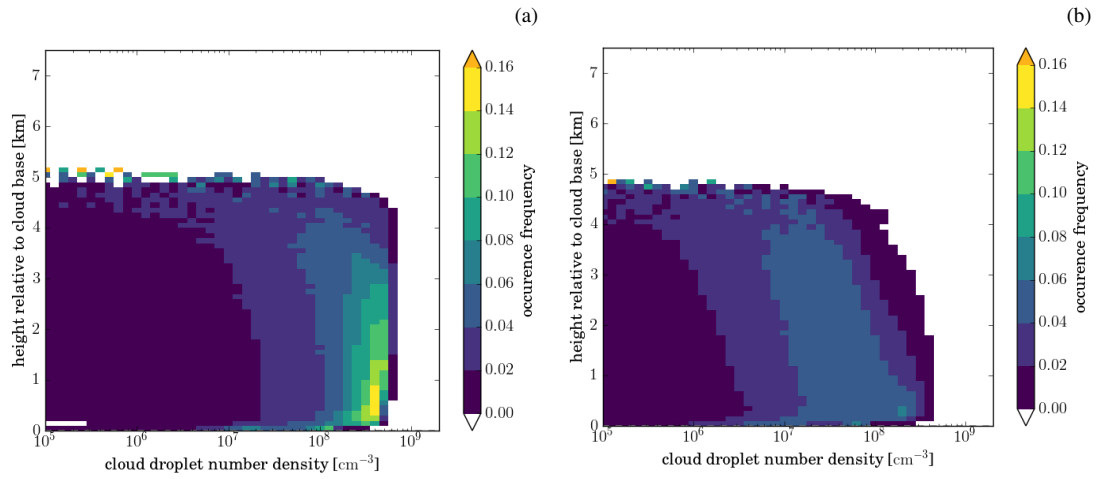


Figure 8. Cloud droplet number concentration from simulations with (a) passive aerosol and (b) aerosol processing as a function of altitude above cloud base. Cloud base is defined as the lowest model level in each column with a cloud droplet mass larger than 1 mg kg^{-1} .

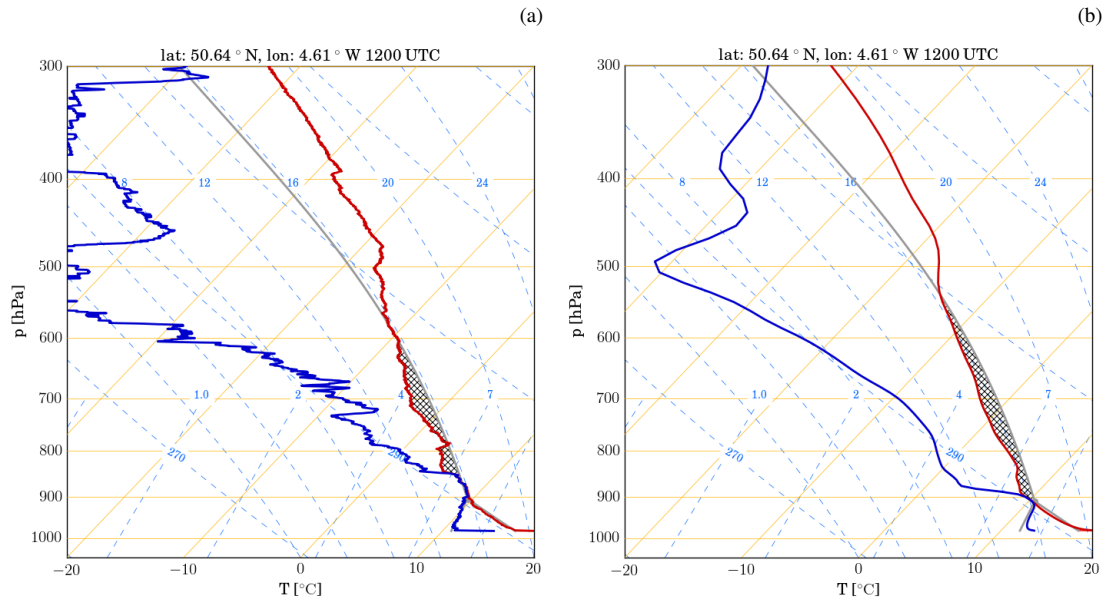


Figure 9. Thermodynamic profiles from (a) radiosonde released at Davidstow at 1200 UTC and (b) the closest grid point in the model for the simulation with the standard aerosol profile and passive aerosols.

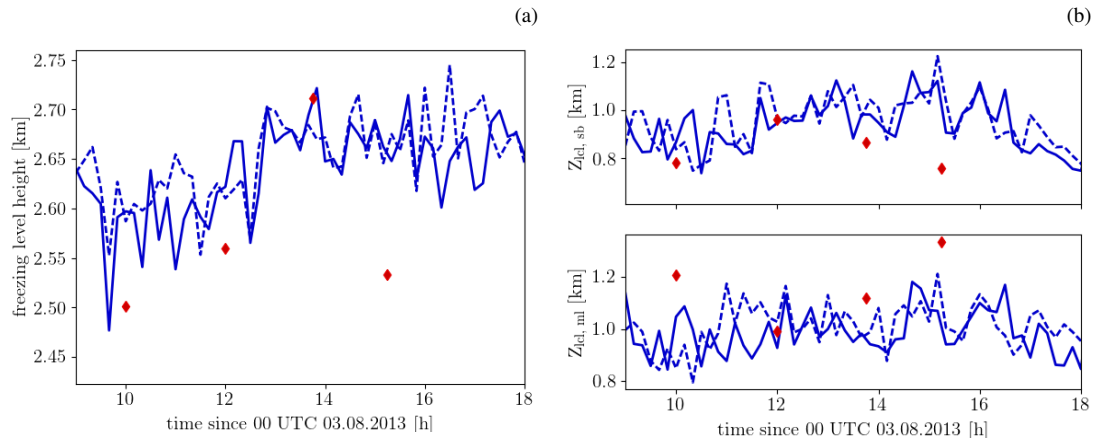


Figure 10. Timeseries of (a) the 0°C level height and (b) the lifting condensation level from the radiosondings at Davidstow (red diamonds) and the closest model gridpoint (blue lines). The lifting condensation level is computed based on air parcels having (i) the thermodynamical properties of the first model level above the surface (upper plot panel b) or (ii) the mean thermodynamical properties of the lowest 50 hPa (lower plot in panel b).

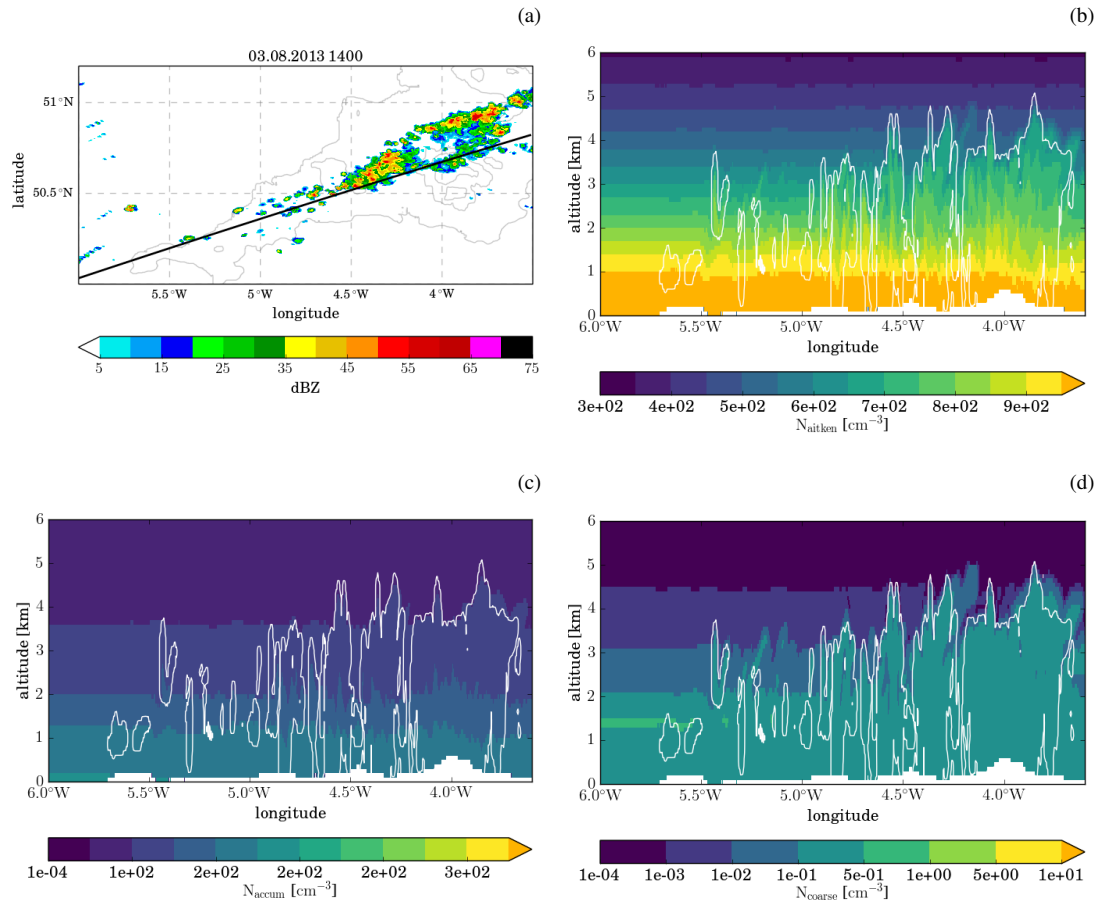


Figure 11. Aerosol fields from the simulation with passive aerosol at 14 UTC. (a) Colour shading shows the column maximum reflectivity and the black line indicates the location of the cross-sections plotted in the other panels: (b) number density of Aitken mode aerosol, (c) accumulation mode aerosol, and (d) coarse mode aerosol. The white contour lines in panels (b) to (d) indicate areas with hydrometeor mixing ratios larger than 1 mg kg^{-1} .

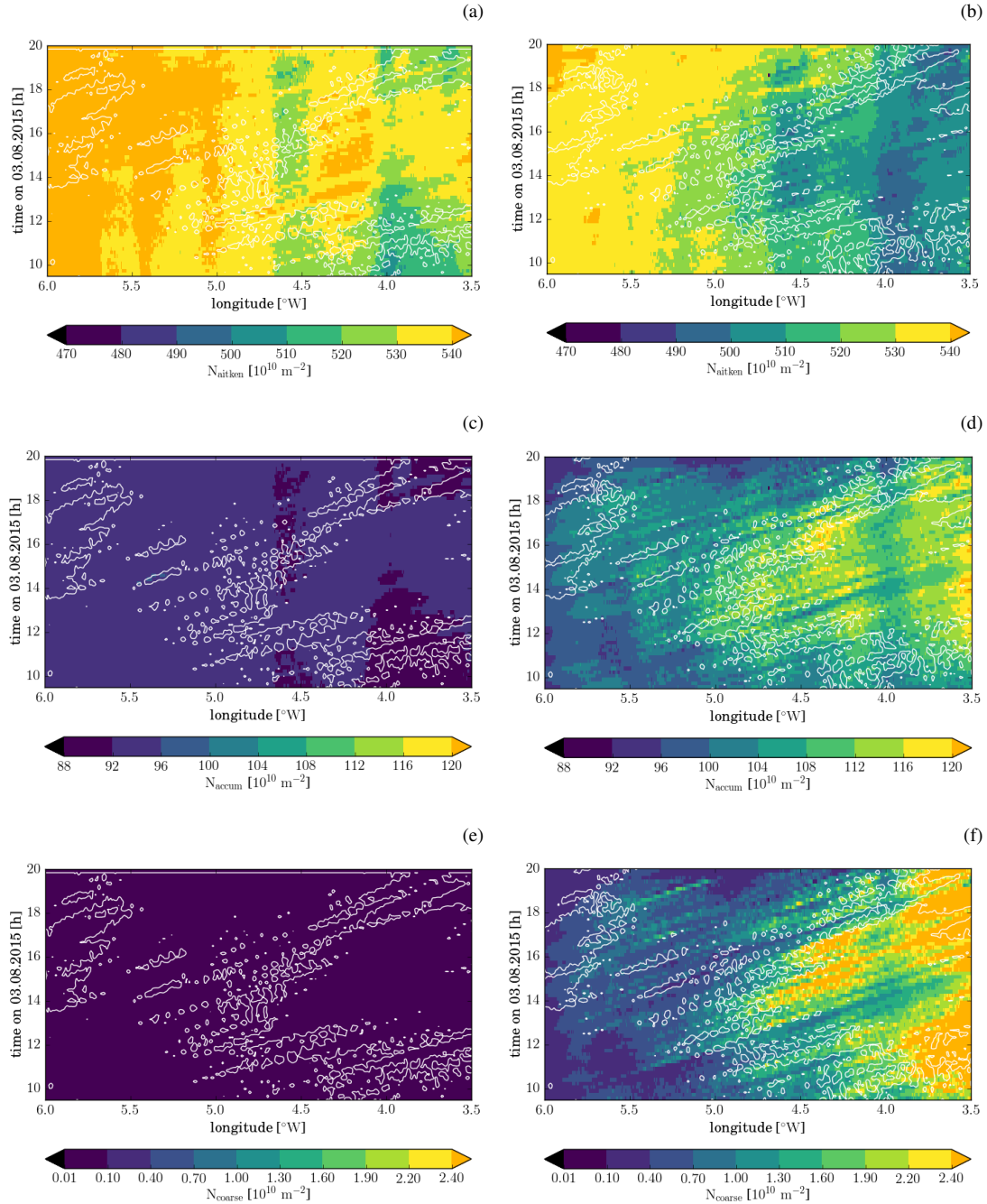


Figure 12. Hovmöller diagrams of latitudinally averaged column integrated aerosol number density from the simulation with passive aerosol (left column) and aerosol processing (right column) and the standard aerosol profile: (a, b) Aitken , (c, d) accumulation, and (e, f) coarse mode. The white contour indicates areas where the condensed water path is larger than 0.1 kg m^{-2} .

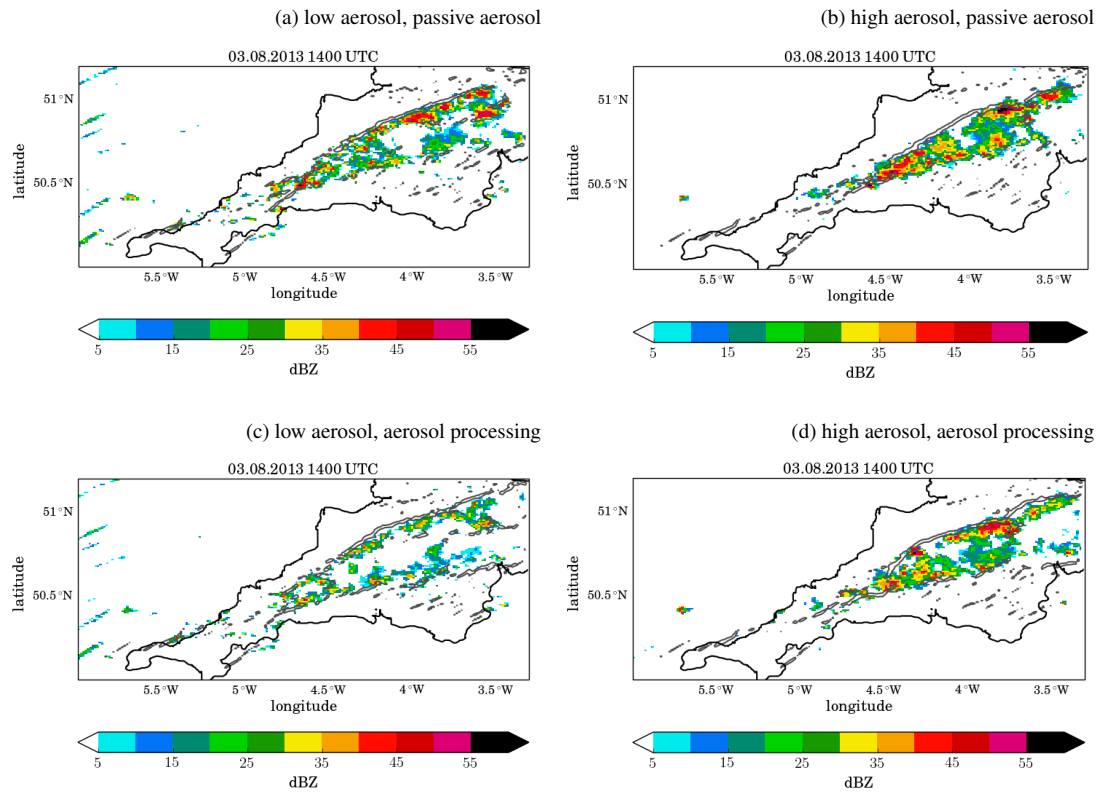


Figure 13. Column maximum radar reflectivity over the COPE domain at 14 UTC from the simulations with (a, b) passive aerosol and (c, d) aerosol processing. The left panels are from simulations with the low aerosol number concentrations and the right panels from those with high aerosol number concentrations.

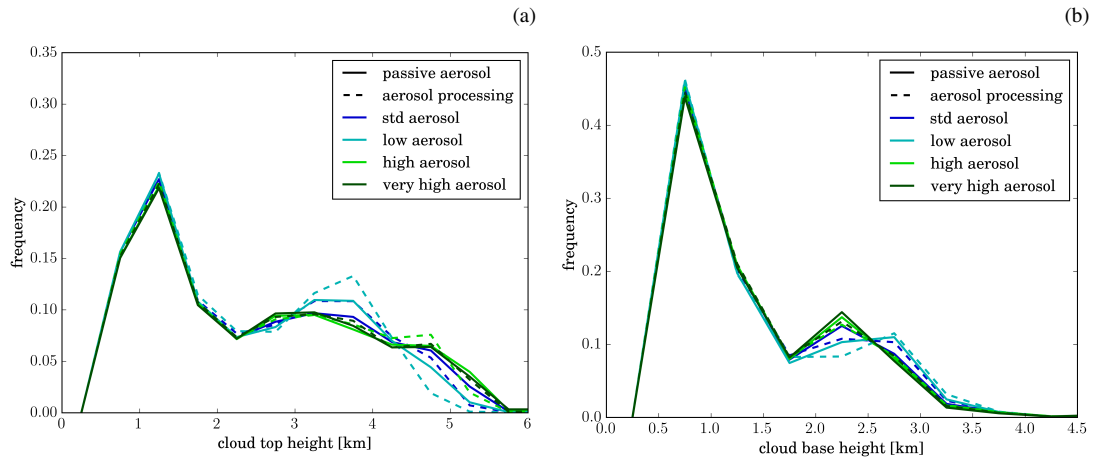


Figure 14. Distribution of (a) cloud top and (b) cloud base height in the different simulations. Cloud top (base) is defined as the highest (lowest) point in each column where the sum of cloud and ice water content exceeds 1 mg kg^{-1} .

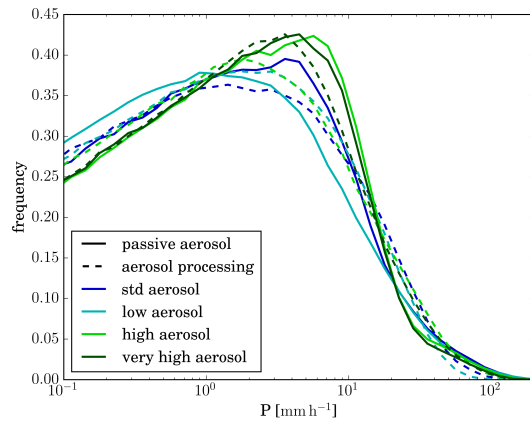


Figure 15. The precipitation rate distribution between 9 UTC and 21 UTC. Different line colours indicate the different aerosol initial conditions, solid lines correspond to simulations with passive aerosols and dashed lines to simulations with aerosol processing.

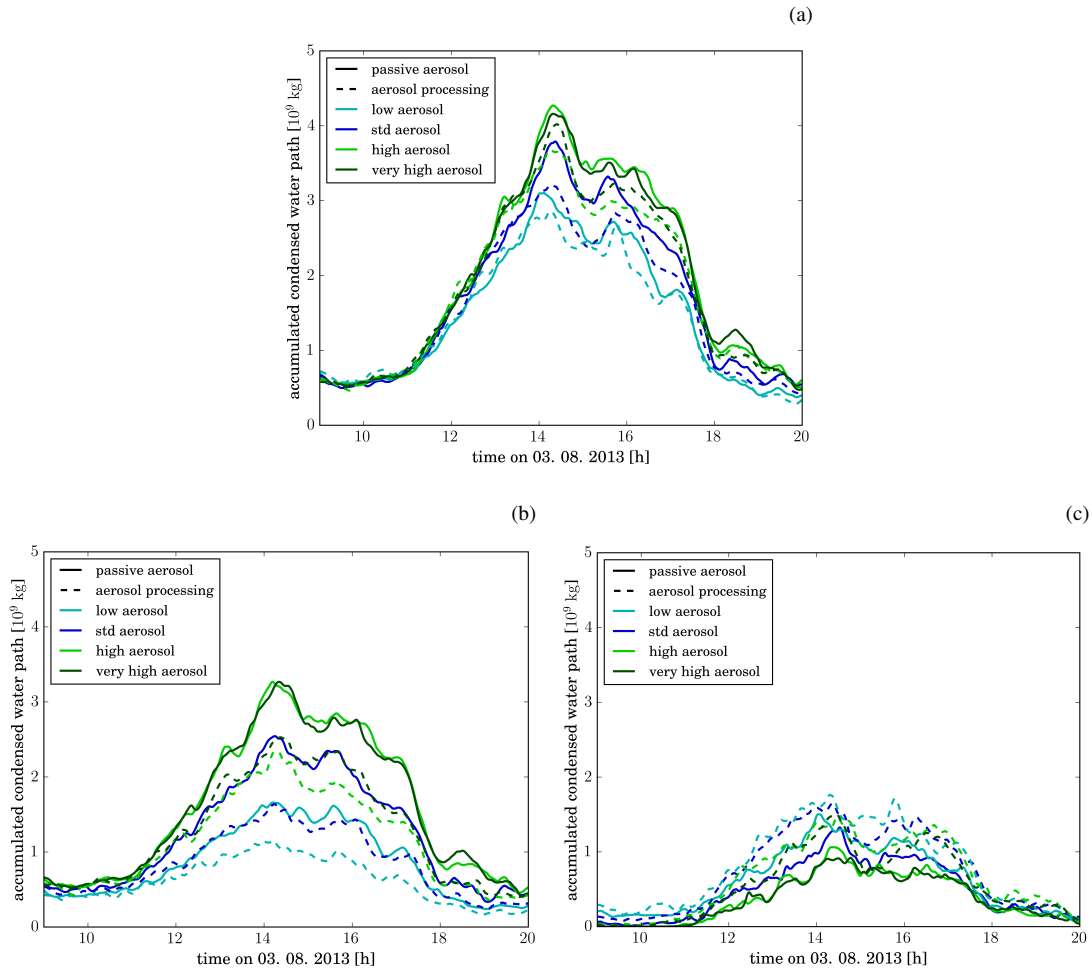


Figure 16. Time evolution of condensed water path in (a) all hydrometeor categories, (b) the cloud, ice and snow categories, and (c) the graupel and rain categories. Different line colours indicate the different aerosol initial conditions, solid lines correspond to simulations with passive aerosols and dashed lines to simulations with aerosol processing.

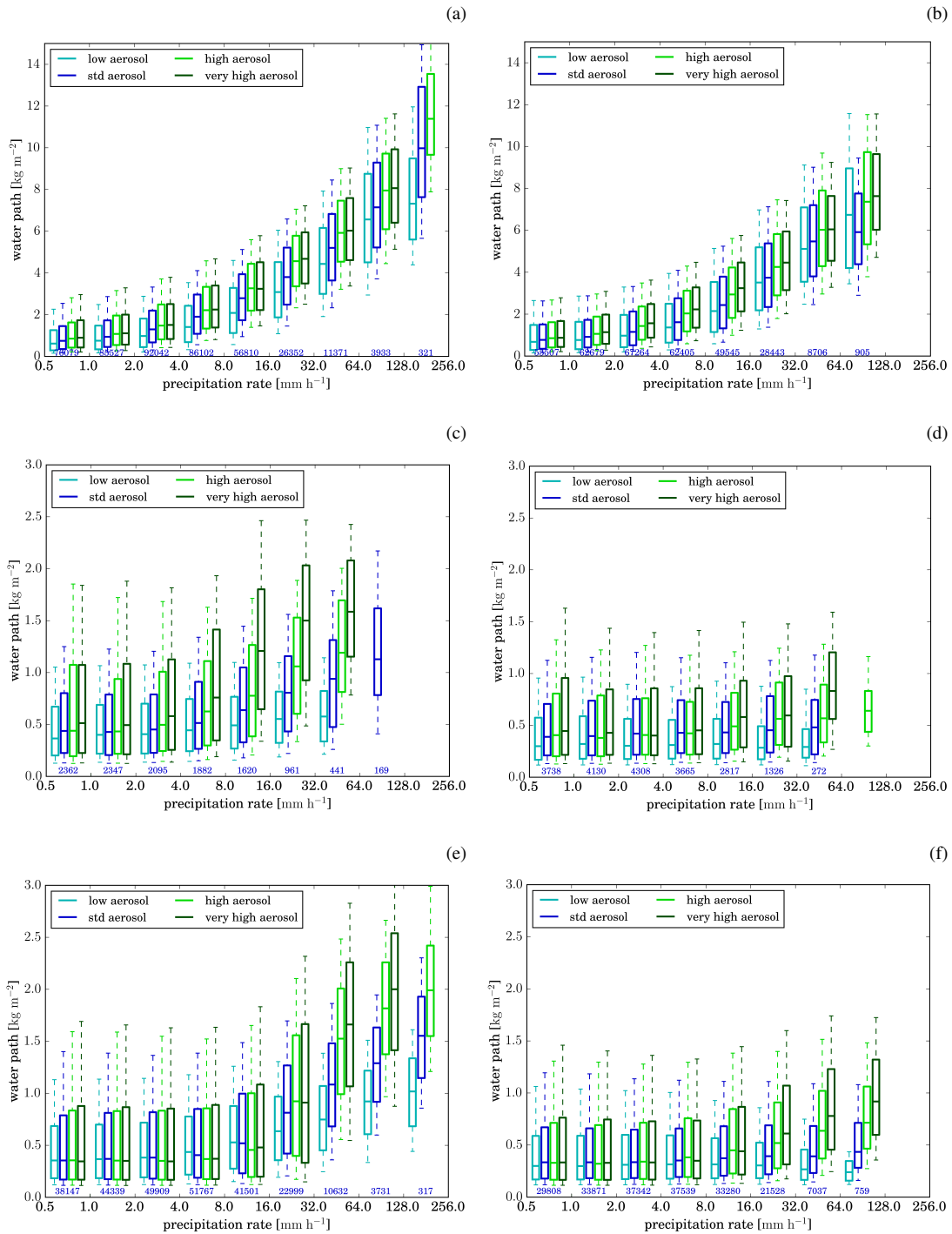


Figure 17. Percentiles of condensed water path (including cloud droplet and ice categories) for the time period between (a, b) 9 - 12 UTC and (c, d) 12 - 20 UTC in columns with certain precipitation rates. (e, f) Percentiles of condensed water path (all hydrometeor categories) in columns with certain precipitation rate for the entire simulation period. The left column shows the simulations with passive aerosol and the right column those with aerosol processing. Different colours correspond to the different aerosol profiles. Values are only shown for precipitation bins with more than 100 data points. The boxes cover the interquartile range (25th to 75th percentile). The whiskers represent the 10th and 90th percentile, respectively. The median water path is shown by the horizontal line in the box

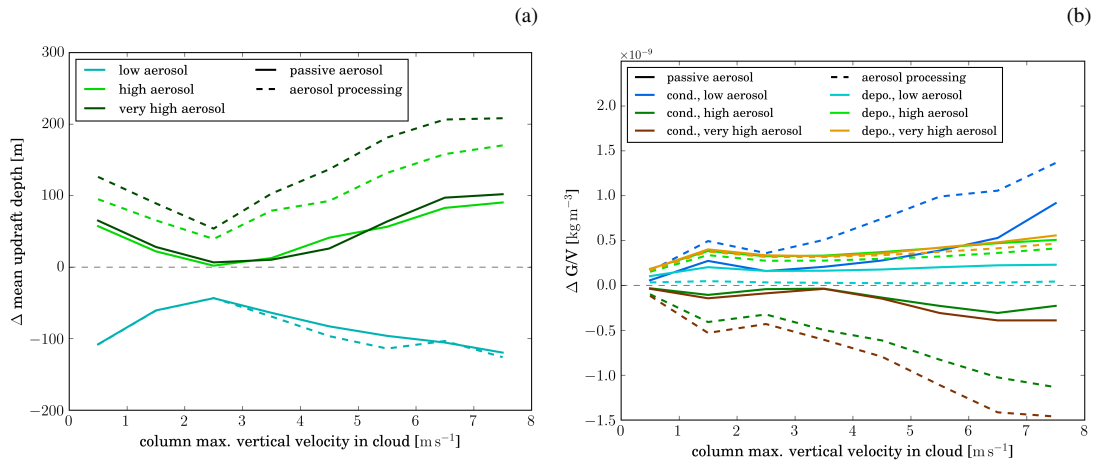


Figure 18. (a) Mean depth of updraft regions ($w > 0 \text{ m s}^{-1}$ and condensate content larger 1 mg kg^{-1}) classified by maximum column in-cloud vertical velocity. (b) Change in mean condensation, evaporation, deposition and sublimation rates for each maximum in-cloud vertical velocity bin. Results from simulations with higher (lower) aerosol loading are depicted in green (blue). Solid lines correspond to simulations with passive aerosol, dashed lines to simulations with aerosol processing.

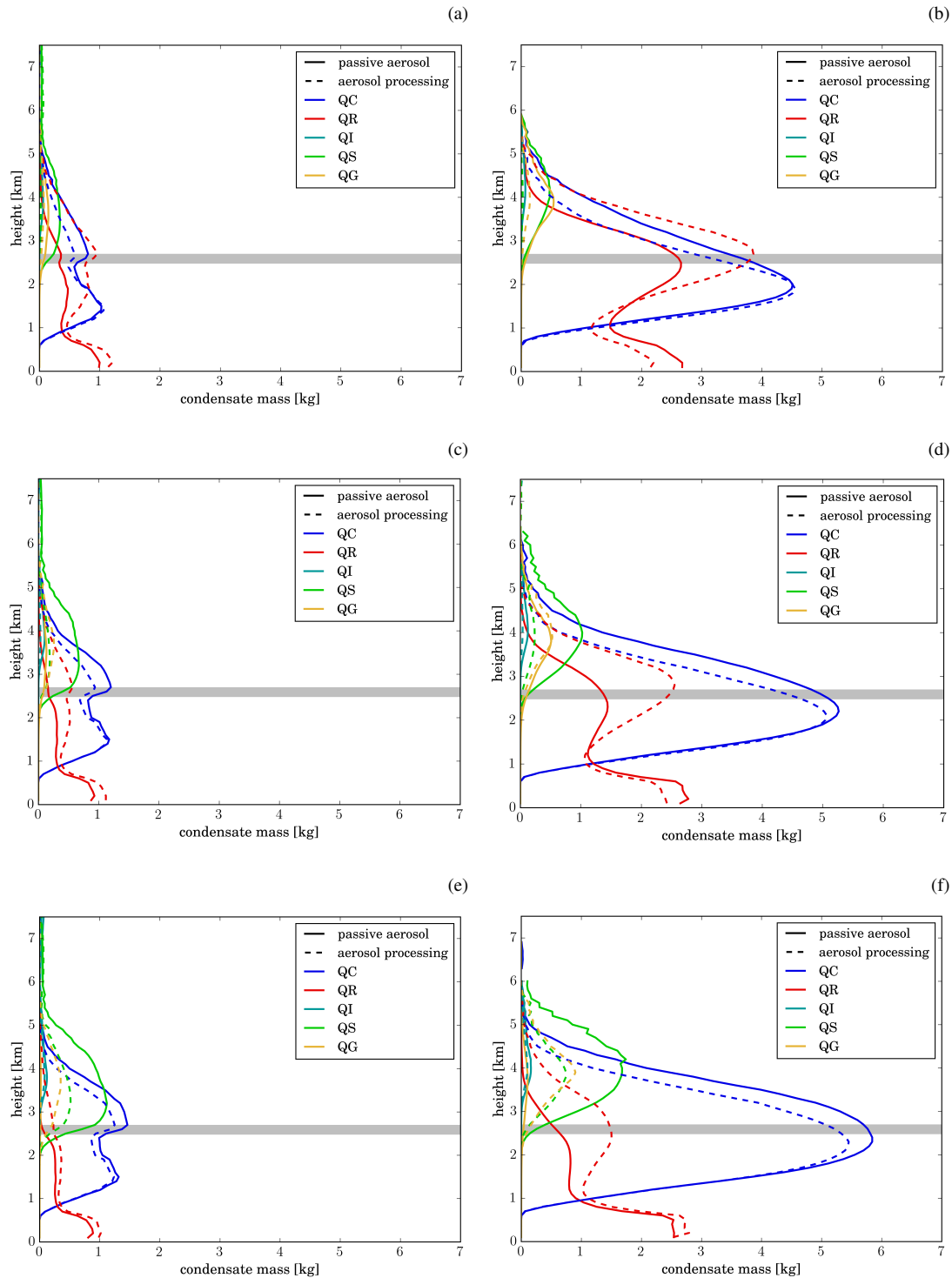


Figure 19. Average profiles of mean mixing ratio of the different hydrometeors (colours) for simulations with (a, b) low, (c, d) standard, and (e, f) high aerosol concentrations. The left panels shows the average over all columns with a column maximum vertical velocity of $0 - 3 \text{ ms}^{-1}$ and the right panels for those with a column maximum vertical velocity larger than 3 ms^{-1} . Solid lines represent simulations with passive aerosols and dashed lines those with aerosol processing. The grey horizontal line indicates the location of the 0°C line in the

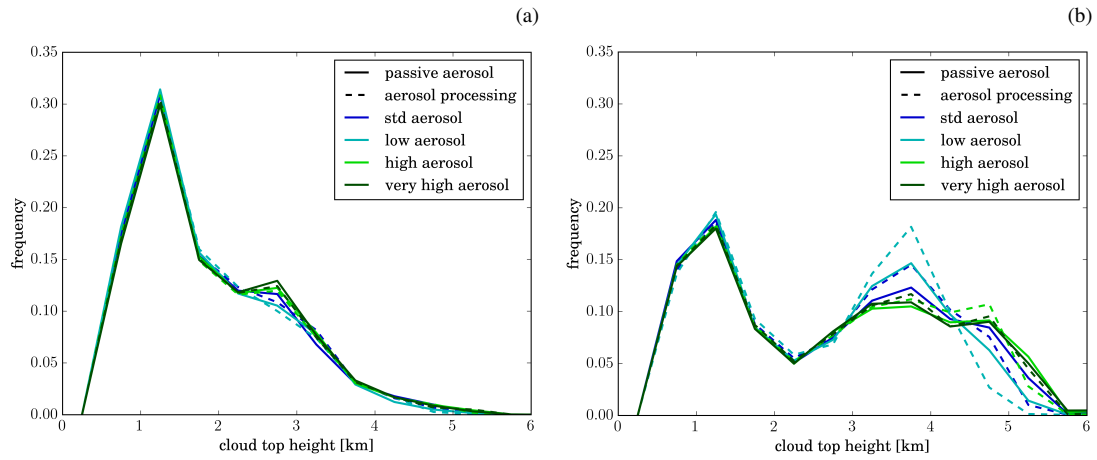


Figure 20. Distribution of cloud top height in the different simulations for the time period between (a) 9 UTC to 12 UTC and (b) 12 UTC to 19 UTC, respectively. Cloud top is defined as the highest point in each column where the condensate content exceeds 1 mg kg^{-1} .

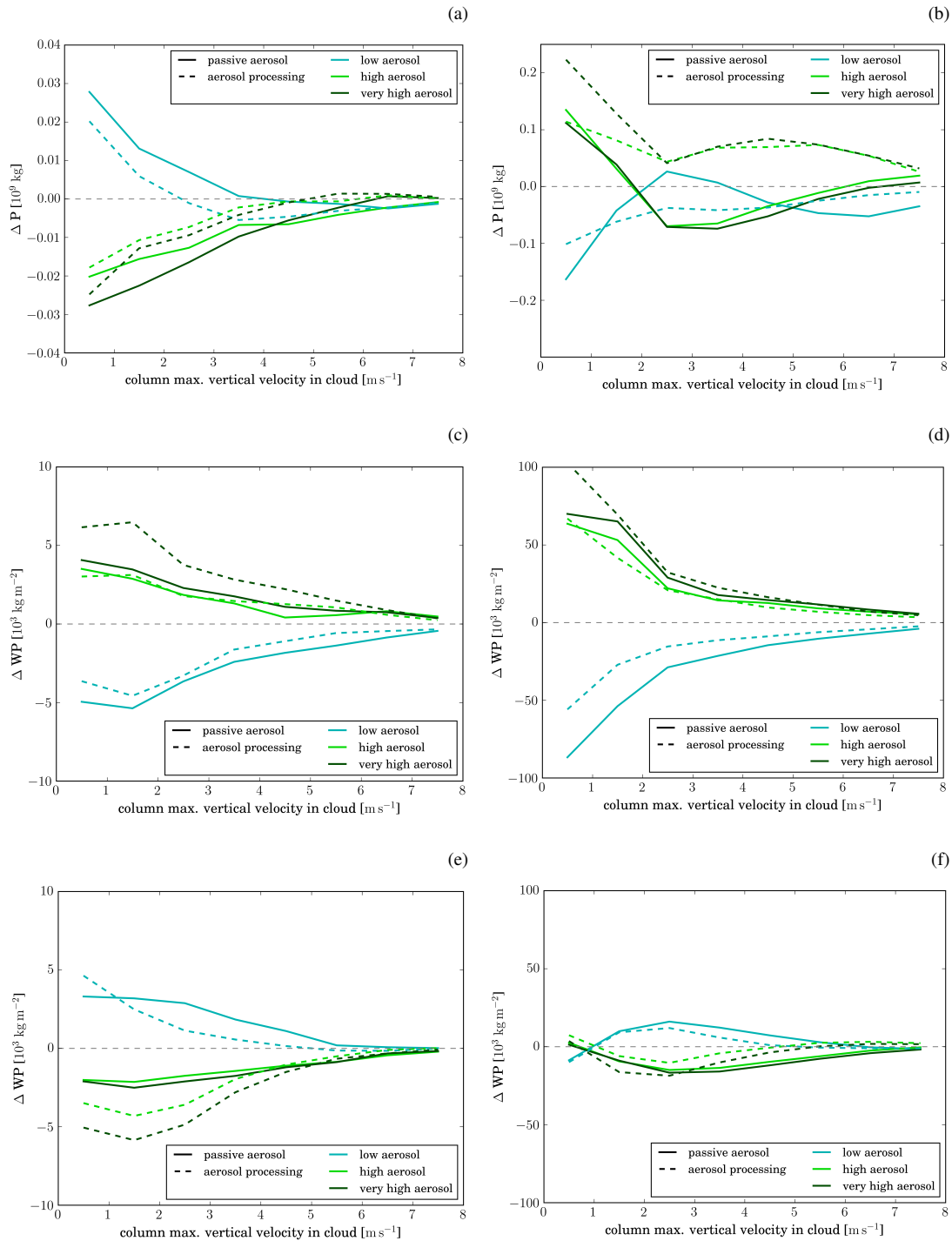


Figure 21. Panels (a, b) show the change in accumulated precipitation relative to the simulations with standard aerosol profile for different w_{\max} . Panels (c, d) show the change in condensed water path including cloud droplets, ice, and snow and (e, f) in the condensed water path including snow rain and graupel. All changes are relative to the simulations with the standard aerosol profile. The panels in the left column are for the time period 9 - 12 UTC and those in the right for for 12 - 20 UTC. Results from simulations with higher (lower) aerosol loading are depicted in green (blue). Solid lines correspond to simulations with passive aerosol, dashed lines to simulations with aerosol processing.